IJRCS

International Journal of Robotics and Control Systems
Vol. 5, No. 3, 2025, pp. 2034-2052
ISSN 2775-2658
http://pubs2.ascee.org/index.php/ijrcs

ASCEE

Indoor Quadcopter Localization Using Fuzzy-Sliding Mode Control for Robust Navigation

Purwadi Agus Darwito [a,1,*], Nilla Perdana Agustina [a,2], Detak Yan Pratama [a,3], Mohammad Naufal Al Farros [a,4], Iwan Cony Setiadi [a,5], Totok Ruki Biyanto [a,6], Choirul Imron [b,7]

[a] Department of Engineering Physics, Institut Teknologi Sepuluh Nopember, Surabaya, Indonesia
[b] Department of Mathematics, Institut Teknologi Sepuluh Nopember, Surabaya, Indonesia
[1] padarwito@ep.its.ac.id; [2] 7009231002@student.its.ac.id; [3] detak@ep.its.ac.id; [4] nalfarros33@gmail.com;
[5] iwancony.setiadi@its.ac.id; [6] trb@ep.its.ac.id; [7] imron-its@matematika.its.ac.id
* Corresponding Author

ARTICLE INFO

Article history
Received May 19, 2025
Revised August 27, 2025
Accepted October 06, 2025

Keywords
Autonomous;
Quadcopter;
Sliding Mode Control;
Fuzzy;
Indoor Localization

ABSTRACT

Growing demand for warehouse automation requires Unmanned Aerial Vehicles (UAVs), particularly quadcopters, to operate autonomously with a high level of precision and reliability. However, indoor localization poses unique challenges due to the absence of Global Positioning System (GPS) signals, making alternative sensors and robust control strategies essential. This study proposes an indoor UAV navigation system that integrates camera and LiDAR sensors with Fuzzy–Sliding Mode Control (Fuzzy-SMC) to enhance stability and reduce the chattering effects commonly associated with Sliding Mode Control. In the proposed method, the camera provides better accuracy for real-time position tracking compared to LiDAR, while fuzzy logic adaptively adjusts the Sliding Mode Control parameters, which serve as the main controller for stabilizing the quadcopter's nonlinear dynamics. Research methodology includes mathematical modeling of the UAV quadcopter, the design of the Fuzzy-SMC controller, and simulation-based testing for trajectory tracking in indoor environments. Results show that the developed system achieves high accuracy, with error values ranging from 0 to 4.044%, remaining below the acceptable threshold of 5%. These findings demonstrate that integration of a camera with Fuzzy-SMC provides an effective and reliable solution for indoor quadcopter UAV navigation, while future research will focus on optimizing the fuzzy rule base and conducting hardware validation in real warehouse scenarios.

1. Introduction

Warehouses play an important role in various industrial sectors as centers for in inventory management and goods distribution [1]-[3]. Efficiency in warehouse management directly affects the operational success of the supply chain [4]-[6]. However, increasing volumes and the complexity of inventory management make manual monitoring inefficient and prone to error [7]-[9]. In addition, workplace hazards such as high storage racks [10]-[12], the use of heavy machinery [13], and the need to monitor large warehouse areas increase the risk to workers [14]-[16]. This challenge underscores the importance of automation technology in improving warehouse safety and operational efficiency [17], [18].

Unmanned Aerial Vehicles (UAVs), particularly quadcopters, have emerged as a promising solution for warehouse automation due to their high maneuverability, reliable performance, and flexibility to operate in confined spaces [19]. This technology enables various applications such as stock monitoring [20], inventory inspection [21], and even automated delivery [22], which were previously carried out using manual methods. With autonomous systems, quadcopters can operate independently without direct control from an operator, thereby not only improving work efficiency but also reducing human involvement in high-risk areas [23]. The autopilot function in quadcopters supports stable and pre-programmed movements, making them highly suitable for the needs of modern warehouses that demand speed and accuracy [24]. In addition, these systems can reduce the risk of workplace accidents, especially in areas that are difficult to access or hazardous for workers. Another advantage is the quadcopter's ability to adapt to dynamic environments, such as avoiding obstacles or automatically adjusting its flight path [25]. Nevertheless, the implementation of quadcopters indoors faces significant challenges, particularly in navigation and localization [26]. This is mainly due to the limitations of Global Positioning System (GPS) signals, which are either unavailable or inaccurate in enclosed spaces, thus requiring alternative and more reliable approaches [27], [28]. This challenge has motivated the advancement of control systems and sensor-based localization methods, such as LiDAR and cameras, to enable quadcopters to operate effectively within warehouse environments [29], [30]. Accordingly, the application of quadcopters in indoor settings should not be regarded merely as a substitute for manual processes, but rather as a critical component of the digital transformation toward smarter and safer warehouse management systems [31], [32]. To address the limitations of GPS in enclosed environments, alternative sensing technologies such as LiDAR and cameras have been introduced [33], [34]. LiDAR provides the capability to reconstruct three-dimensional maps of the surroundings, whereas cameras offer real-time visual information to facilitate position tracking and spatial reconstruction [35], [36]. Nevertheless, sensor-based localization alone remains insufficient, as quadcopters inherently require robust control algorithms to ensure trajectory stability and reliable autonomous navigation. Recent studies have proposed a variety of indoor localization approaches that integrate sensors with advanced control algorithms, including visual odometry, sensor fusion, and the deployment of external camera systems [37]-[39]. However, these approaches continue to encounter several limitations, such as high implementation costs, restricted operational coverage, and reduced effectiveness in coping with uncertainties in dynamic warehouse environments [40]-[42].

The success of indoor quadcopter navigation is not determined solely by sensors, but is highly dependent on the control system employed [43], [44]. Control algorithms play a crucial role in maintaining quadcopter stability, regulating trajectory tracking, and ensuring autonomous operation within complex warehouse environments [45]. Therefore, research on indoor localization cannot be separated from the development of control methods that are both adaptive and robust against disturbances and environmental uncertainties. The indoor localization system integrating an Inertial Measurement Unit (IMU) and Ultra-Wideband (UWB) sensors is developed using the Extended Kalman Filter control method. Experimental results demonstrate its effectiveness in achieving accurate 3D positioning and yaw estimation [46]. A model-based reinforcement learning (RL) approach is proposed to enable UAVs to navigate and make autonomous decisions in environments without GNSS and with limited visibility. The proposed architecture integrates onboard sensors, including a thermal camera to detect trapped victims (targets), a 2D LiDAR, and an IMU for localization. Experimental results demonstrate high success rates in target detection as well as robust performance in obstacle avoidance and navigation, despite uncertainties in pose estimation and detection [47]. The UAV system has a complex model and the Sliding Mode Control (SMC) method is known for its robustness against model inaccuracies and external disturbances [48]-[50]. The study employs Sliding Mode Control (SMC) combined with disturbance observers across the six degrees of freedom of the quadcopter to effectively reject external disturbances. While ensuring stability conditions, all control parameters were automatically initialized and tuned using a simulation-based offline Particle Swarm Optimization (PSO) algorithm, followed by onboard manual fine-tuning [51].

However, SMC still has a fundamental drawback in the form of the chattering phenomenon, which refers to high-frequency oscillations arising from the switching mechanism in the control law [52]. This effect not only degrades system performance but also has the potential to cause instability, excessive

energy consumption, and premature actuator wear. Several methods have been proposed to mitigate the chattering phenomenon, introduces a chattering-free terminal sliding mode control approach for chaotic systems with unknown uncertainties. The method combines SMC with adaptive control to address the upper bound of model uncertainties without increasing control gains, by employing an adaptive continuous barrier function [53]. A boundary logic-based hybrid scheme that combines SMC and Proportional Integral Derivative (PID) controllers is proposed for underactuated nonlinear systems. While PID is effective for linear systems, it lacks robustness over a wide operating range, whereas SMC offers high robustness but suffers from chattering issues and practical implementation challenges. To address these limitations, a boundary-based adaptive exponential reaching law is developed to enhance the effectiveness of SMC [54]. Fuzzy Logic Control (FLC) has begun to be widely combined with SMC to adaptively adjust control parameters. FLC provides nonlinear decision-making capabilities that can reduce chattering effects while maintaining system robustness [55]-[57]. However, research integrating Fuzzy–SMC for quadcopter navigation and localization within warehouses or indoor remains limited. Previous studies have largely relied on camera-based localization systems, which are expensive and impractical for large-scale warehouses, or have focused solely on basic stabilization without considering the challenges of indoor navigation.The contributions of this research are as follows:

- Developing a quadcopter navigation control system for indoor localization in warehouses using Fuzzy–SMC to reduce chattering and improve system robustness;
- Conducting a comparative evaluation between LiDAR and camera sensors for indoor localization accuracy, thereby providing insight into their effectiveness in warehouse environments.

2. Material and Control Design

2.1. Quadcopter Mathematical Model

The quadcopter mission profile represents the flight stages designed to test and optimize the performance of the quadcopter's control system and stability [58]. Based on Fig. 1, this study involves a quadcopter flight mission that includes taking off, hovering, cruising, hovering again, and finally landing. Before take-off, the quadcopter is stationary with all four rotors inactive. During take-off, all four rotors spin at the same speed, generating upward lift and causing the quadcopter to ascend. Once it reaches a pre-determined altitude, the four rotors will rotate at a constant speed. When the quadcopter performs cruising, the two rotors at the front of the quadcopter will decrease their speed, while the two rear rotors will increase their speed, generating forward thrust. Once it reaches the designated point, the quadcopter must enter a hovering state, where the speed of all four rotors is maintained at a constant level. Afterward, the quadcopter will gradually reduce the speed of its rotors, thereby decreasing the lift generated by the rotor rotation, allowing the quadcopter to descend back to the ground. Once it reaches the ground, all four rotors will stop, and the quadcopter will have successfully landed at the designated point.

The implementation in Fig. 1 an autonomous system on a quadcopter enhances the effectiveness and efficiency of its predetermined flight path before the flight mission. Although it has 6 equations of motion, the quadcopter is a dynamic system with 4 inputs (z, ϕ, θ, ψ), as there are 4 motors driving the quadcopter, as shown in Fig. 2.

The relationship between rotational motion and translational motion in the body frame is expressed in R matrix [59].

$$\mathrm{R} = \begin{bmatrix} \cos\psi\cos\theta & \cos\psi\sin\theta\sin\phi - \sin\psi\cos\phi & \cos\psi\sin\theta\cos\phi + \sin\psi\sin\phi \\ \sin\psi\cos\theta & \sin\psi\sin\theta\sin\phi + \sin\psi\cos\phi & \sin\psi\sin\theta\cos\phi - \cos\psi\sin\phi \\ -\sin\theta & \cos\theta\sin\phi & \cos\theta\cos\phi \end{bmatrix} \quad (1)$$

The most commonly used mathematical model to represent the dynamics of a quadcopter is the Euler-Newton model, which is based on Newton's and Euler's laws. This model takes into account

velocity, acceleration, moment of inertia, aerodynamic forces, and the torque applied to the quadcopter. The external forces acting on each axis are represented in (2).

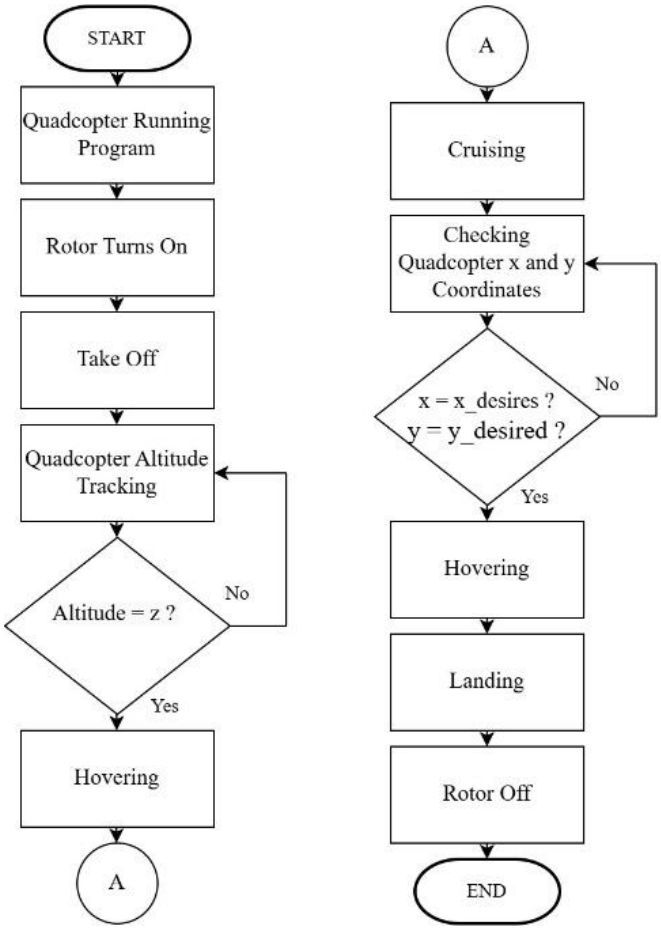

Fig. 1. Flowchart of quadcopter flight mission

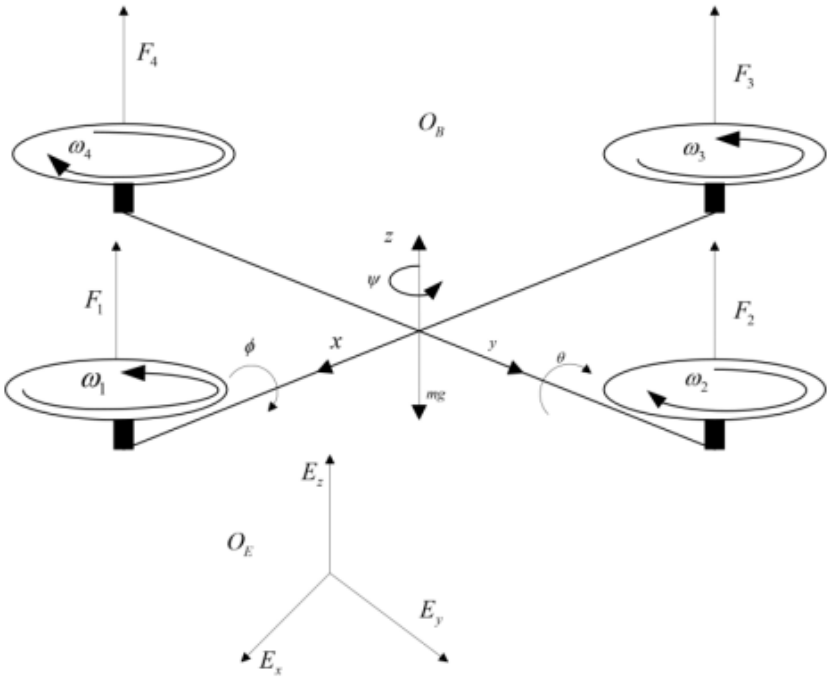

Fig. 2. Force on quadcopter

$$\begin{aligned} F_x &= m(w - rv + \dot{u}) \\ F_y &= m(-(pw - ru) + \dot{v}) \\ F_z &= m(pv - qu + \dot{w}) \end{aligned} \tag{2}$$

Because the propellers rotate in opposite directions, the quadcopter will remain stable, and the torque or moment will be balanced. Since the aerodynamic and gyroscopic torques cancel each other out when the UAV quadcopter is flying in a static condition, the moment of the quadcopter (M) in the x, y, and z directions can be derived, and the mathematical model is expressed as shown in (3).

$$\begin{aligned} \ddot{\phi} &= \frac{l}{I_x}U_2 + \frac{I_y}{I_x}\dot{\theta}\dot{\psi} - \frac{I_z}{I_x}\dot{\theta}\dot{\psi} \\ \ddot{\theta} &= \frac{l}{I_y}U_3 + \frac{I_z}{I_y}\dot{\phi}\dot{\psi} - \frac{I_x}{I_y}\dot{\phi}\dot{\psi} \\ \ddot{\psi} &= \frac{l}{I_z}U_4 + \frac{I_x}{I_z}\dot{\phi}\dot{\theta} - \frac{I_y}{I_z}\dot{\phi}\dot{\theta} \\ \ddot{x} &= \frac{U_1}{m}(\cos\psi\sin\theta\cos\phi + \sin\psi\sin\phi) \\ \ddot{y} &= \frac{U_1}{m}(\sin\psi\sin\theta\cos\phi - \cos\psi\sin\phi) \\ \ddot{z} &= g + \frac{U_1}{m}(\cos\theta\cos\phi) \end{aligned} \tag{3}$$

The information regarding the relationship between the control signals and the angular velocity of the four rotors is presented in (4).

$$\begin{aligned} \omega_1^2 &= \frac{U_1}{4b} - \frac{U_2}{2bl} - \frac{U_4}{4d} \\ \omega_2^2 &= \frac{U_1}{4b} - \frac{U_3}{2bl} + \frac{U_4}{4d} \\ \omega_3^2 &= \frac{U_1}{4b} + \frac{U_2}{2bl} - \frac{U_4}{4d} \\ \omega_4^2 &= \frac{U_1}{4b} + \frac{U_3}{2bl} + \frac{U_4}{4d} \end{aligned} \tag{4}$$

2.2. Control System

SMC consists of two different parts, namely the sliding surface and the control law. The sliding surface is the part that deals with designing the sliding conditions to produce characteristics that are suitable for design. In addition, this part also represents a numerical function that produces characteristics suitable for design [60]. The mathematical equation for SMC is generally written in (5).

$$\begin{aligned} \sigma &= \mathrm{f}(\mathrm{e}, \mathrm{e}, \ldots, e^k) \\ \sigma &= e^k + \sum_{i=0}^{k-1} Ci + e^i \\ \sigma &= (\frac{d}{dt} + p)^k e \end{aligned} \tag{5}$$

Control law is the part to decide the control law that will be applied to the system later, the equation is written in (6).

$$\mu = -U * sgn(\sigma) \tag{6}$$

In the Sliding Mode Control (SMC) control system, it is necessary to determine the sliding surface in equation (7) to control the quadcopter. Here is the sliding surface that will be applied to the quadcopter [61].

$$\begin{aligned} s_x &= \dot{e}_x + \lambda_x e_x \\ s_y &= \dot{e}_y + \lambda_y e_y \\ s_z &= \dot{e}_z + \lambda_z e_z \\ s_\phi &= \dot{e}_\phi + \lambda_\phi e_\phi \\ s_\theta &= \dot{e}_\theta + \lambda_\theta e_\theta \\ s_\psi &= \dot{e}_\psi + \lambda_\psi e_\psi \end{aligned} \tag{7}$$

To ensure the stability of the system, $\dot{V}_x < 0$, so the sliding mode condition applied is written in (8).

$$\dot{s}_x = -k_{1_x} sign(s_x) - k_{2_x} s_x \tag{8}$$

However, if the determination of the sliding surface value is not appropriate, it will cause a chattering effect. The chattering effect occurs when there are oscillations on the sliding surface, so that it will produce a discontinuous trajectory [62].

2.2.1. Fuzzy Controller

In the design of the Fuzzy control system, Fuzzy logic functions as a tuning mechanism for the SMC parameters, thereby determining the values of k_{1_x}, k_{2_x}, k_{1_y}, k_{2_y}, k_{1_z}, k_{2_z}, k_{1_ϕ}, k_{2_ϕ}, k_{1_θ}, k_{2_θ}, k_{1_ψ}, $and\ k_{2_\psi}$. The design of the Fuzzy control system begins with the construction of the membership functions and the rule base. In developing the membership functions, the input and output variables to be used must first be specified.

The membership functions on each axis are defined according to Table 1 for the x-axis, Table 2 for the y-axis and z-axis membership functions, along with the fuzzy sets and ranges for each input and output variable. Each fuzzy category is designed to correspond with the desired conditions. For instance, when the error value is very large, as shown in Table 1, the Negative High (NH) category corresponds to an error value of –90 and a delta error of –75, resulting in an output ranging from 0.00825 to 0.0115. This output is then mapped to the rule base presented in Table 6. Specifically, when the error value falls under the NH (Negative High) category and the delta error also belongs to the NH (Negative High) category, the system produces a PH (Positive High) output. Table 3 presents the membership functions for the ϕ axis, including the fuzzy sets and the ranges for each input and output variable. The membership function for the input variable of the θ position error is shown in Table 4. For the ψ axis fuzzy system, the membership function domains are derived from Table 5.

Then, after determining the membership function ranges for both input and output variables, the next step is to define the system rule base for gain determination, as presented in Table 6. In the actual implementation for example on the x-axis, the input variables are the position error in x and the delta x error, which represent the difference between the desired and actual quadcopter positions. Meanwhile, the output variable k_x corresponds to the SMC gain value, which ultimately affects the rotor speed. The use of Fuzzy categories such as NH, NM, NL, Z, PL, PM, and PH facilitates smoother and more flexible mapping of input values to outputs compared to traditional control methods. The membership functions shown in the figure illustrate how the Fuzzy inference system maps numerical input values into Fuzzy categories. This is crucial to ensure that every flight condition can be properly detected and handled. For instance, the “NH” category for highly negative

"X" values indicates a condition that requires rapid corrective action to avoid instability. In this case, Sliding Mode Control will be implemented in parallel with Fuzzy logic to tune the SMC gain parameters.

Table 1. Membership function domain of the X axis

No	Membership Function	Input Variables		Output Variables
		Error x(m)	Error rate x(m/s)	Throttle
1	Negative High (NH)	[-90 -55 -45 -30]	[-75 -60 -45 -30]	[0.0001 0.0005 0.0015 0.00275]
2	Negative Medium (NM)	[-45 -30 -15]	[-45 -30 -15]	[0.0015 0.00275 0.004]
3	Negative Low (NL)	[-30 -15 0]	[-30 -15 0]	[0.00275 0.004 0.00525]
4	Zero (Z)	[-5 0 5]	[-10 0 10]	[0.00475 0.0055 0.00625]
5	Positive Low (PL)	[0 15 30]	[0 15 30]	[0.00575 0.007 0.00825]
6	Positive Medium (PM)	[15 30 45]	[15 30 45]	[0.007 0.00825 0.0095]
7	Positive High (PH)	[30 45 55 90]	[30 45 60 75]	[0.00825 0.0095 0.0105 0.0115]

Table 2. Membership function domain of the Y and Z axis

No	Membership Function	Input Variables		Output Variables
		Error x(m)	Error rate x(m/s)	Throttle
1	Negative High (NH)	[-90 -60 -45 -30]	[-75 -60 -45 -30]	[0.0001 0.0005 0.0015 0.00275]
2	Negative Medium (NM)	[-45 -30 -15]	[-45 -30 -15]	[0.0015 0.00275 0.004]
3	Negative Low (NL)	[-30 -15 0]	[-30 -15 0]	[0.00275 0.004 0.00525]
4	Zero (Z)	[-10 0 10]	[-5 0 5]	[0.00475 0.0055 0.00625]
5	Positive Low (PL)	[0 15 30]	[0 15 30]	[0.00575 0.007 0.00825]
6	Positive Medium (PM)	[15 30 45]	[15 30 45]	[0.007 0.00825 0.0095]
7	Positive High (PH)	[30 45 60 90]	[30 45 60 75]	[0.00825 0.0095 0.0105 0.0115]

Table 3. Membership function domain of the ϕ axis

No	Membership Function	Input Variables		Output Variables
		Error x(m)	Error rate x(m/s)	Throttle
1	Negative High (NH)	[-70.25 -60.25 -40.25 -30.25]	[-20 -15 5 10]	[0.0001 0.0005 0.0015 0.00275]
2	Negative Medium (NM)	[-40.25 -30.25 -20.25]	[5 10 15]	[0.0015 0.00275 0.004]
3	Negative Low (NL)	[-30.25 -20.25 -10.25]	[10 15 20]	[0.00275 0.004 0.00525]
4	Zero (Z)	[-10.25 0 10.25]	[20 24 28]	[0.00475 0.0055 0.00625]
5	Positive Low (PL)	[10.25 20.25 30.25]	[28 33 38]	[0.00575 0.007 0.00825]
6	Positive Medium (PM)	[20.2 30.2 40.2]	[33 38 43]	[0.007 0.00825 0.0095]
7	Positive High (PH)	[30.25 40.25 60.25 70.25]	[38 43 63 68]	[0.00825 0.0095 0.0105 0.0115]

Table 4. Membership function domain of the θ axis

No	Membership Function	Input Variables		Output Variables
		Error x(m)	Error rate x(m/s)	Throttle
1	Negative High (NH)	[-70.25 -60.25 -40.25 -30.25]	[-5 -2 2 5]	[0.0001 0.0005 0.0015 0.00275]
2	Negative Medium (NM)	[-40.25 -30.25 -20.25]	[2 5 8]	[0.0015 0.00275 0.004]
3	Negative Low (NL)	[-30.25 -20.25 -10.25]	[5 8 11]	[0.00275 0.004 0.00525]
4	Zero (Z)	[-10.25 0 10.25]	[11 15.5 20]	[0.00475 0.0055 0.00625]
5	Positive Low (PL)	[10.25 20.25 30.25]	[20 23 26]	[0.00575 0.007 0.00825]
6	Positive Medium (PM)	[20.2 30.2 40.2]	[23 26 29]	[0.007 0.00825 0.0095]
7	Positive High (PH)	[30.25 40.25 60.25 70.25]	[26 29 33 36]	[0.00825 0.0095 0.0105 0.0115]

Table 5. Membership function domain of the ψ axis

No	Membership Function	Input Variables		Output Variables
		Error x(m)	Error rate x(m/s)	Throttle
1	Negative High (NH)	[-120 -100 -80 -60]	[-5 -2 2 5]	[0.0001 0.0005 0.0015 0.00275]
2	Negative Medium (NM)	[-80 -60 -40]	[2 5 8]	[0.0015 0.00275 0.004]
3	Negative Low (NL)	[-60 -40 -20]	[5 8 11]	[0.00275 0.004 0.00525]
4	Zero (Z)	[-20 0 20]	[11 15.5 20]	[0.00475 0.0055 0.00625]
5	Positive Low (PL)	[20 40 60]	[20 23 26]	[0.00575 0.007 0.00825]
6	Positive Medium (PM)	[40 60 80]	[23 26 29]	[0.007 0.00825 0.0095]
7	Positive High (PH)	[60 80 100 120]	[26 29 33 36]	[0.00825 0.0095 0.0105 0.0115]

Table 6. Rule base of the controller

Error	Error derivatif						
	NH	NM	NL	Z	PL	PM	PH
NH	PH	PH	PH	PH	PM	PL	Z
NM	PH	PH	PH	PM	PL	Z	NL
NL	PH	PH	PM	PL	Z	NL	NL
Z	PH	PM	PL	Z	NL	NL	NM
PL	PM	PL	Z	NL	NL	NM	NH
PM	PL	Z	NL	NL	NM	NM	NH
PH	Z	NL	NL	NM	NM	NH	NH

In this research, based on Fig. 3, Fuzzy Logic is used to tune the SMC gain according to the desired conditions. The use of Fuzzy Logic will change the SMC gain value according to the changing conditions that occur. Thus, the quadcopter remains in the sliding surface condition and does not experience the chattering effect. The combination of these two methods will allow the quadcopter to fly in a stable and accurate condition when flying missions. Thus, the use of Fuzzy and SMC will help to provide stability in the movement of the quadcopter. The autonomous control system on the quadcopter is implemented by using a trajectory equation that is set in such a way that it can run according to the desired flying mission. In performing indoor localization, the quadcopter will run according to the specified trajectory. However, to validate the position of the quadcopter, sensors are required. In this research, two sensors are used to compare their performance in reading the position accurately. First, a LiDAR sensor is used and the second is a camera. Tests were carried out by performing two variations of the trajectory equation:

- Trajectory I_A

$$x_d(t) = \begin{cases} 0, & 0 \le t < 10 \\ \frac{1}{6}(t-10), & 10 \le t < 40 \\ 5, & 40 \le t \le 100 \end{cases}$$
$$y_d(t) = \begin{cases} 0, & 0 \le t < 10 \\ 0, & 10 \le t < 40 \\ \frac{1}{6}(t-40), & 40 \le t \le 100 \end{cases} \quad (9)$$
$$z_d(t) = \begin{cases} 0.15t, & 0 \le t < 10 \\ 1.5, & 10 \le t < 40 \\ 1.5, & 40 \le t \le 100 \end{cases}$$

- Trajectory I_B

$$x_d(t) = \begin{cases} 0, & 0 \le t < 18 \\ \frac{5}{26}(t-18), & 18 \le t < 44 \\ 5, & 44 \le t \le 100 \end{cases} \quad (10)$$

$$y_d(t) = \begin{cases} 0, & 0 \le t < 18 \\ 0, & 18 \le t < 44 \\ \frac{5}{28}(t-44), & 44 \le t \le 100 \end{cases}$$

$$z_d(t) = \begin{cases} 0.25t, & 0 \le t < 18 \\ 4.5, & 18 \le t < 44 \\ 4.5, & 44 \le t \le 100 \end{cases}$$

2.2.2. Design Converter

At a certain altitude, the quadcopter performs altitude sensing, resulting in a z-position error, which is then fed back to the altitude control. As a result, the altitude control equation is represented as shown in (4).

$$\ddot{z} = g + \frac{U_1}{m}$$
$$U_1 = m\,(\ddot{z} + g) \tag{11}$$

Value of U_1 represents the lift force generated by the throttle for altitude control. Additionally, modeling is also performed to determine the input in terms of x and y positions. In this case, the angles that have an effect are the roll and pitch angles.

$$\begin{bmatrix} \phi_{desired} \\ \theta_{desired} \end{bmatrix} = \frac{m}{U_1} \begin{bmatrix} \cos\psi & \sin\psi \\ \sin\psi & -\cos\psi \end{bmatrix} \begin{bmatrix} \ddot{x} \\ \ddot{y} \end{bmatrix} \tag{12}$$

The $\phi_{desired}$ value is the desired value of the angular position ϕ due to the desired value of the x axis position. While the $\theta_{desired}$ value is the desired value of the angular position θ due to the desired value of the y axis position [59].

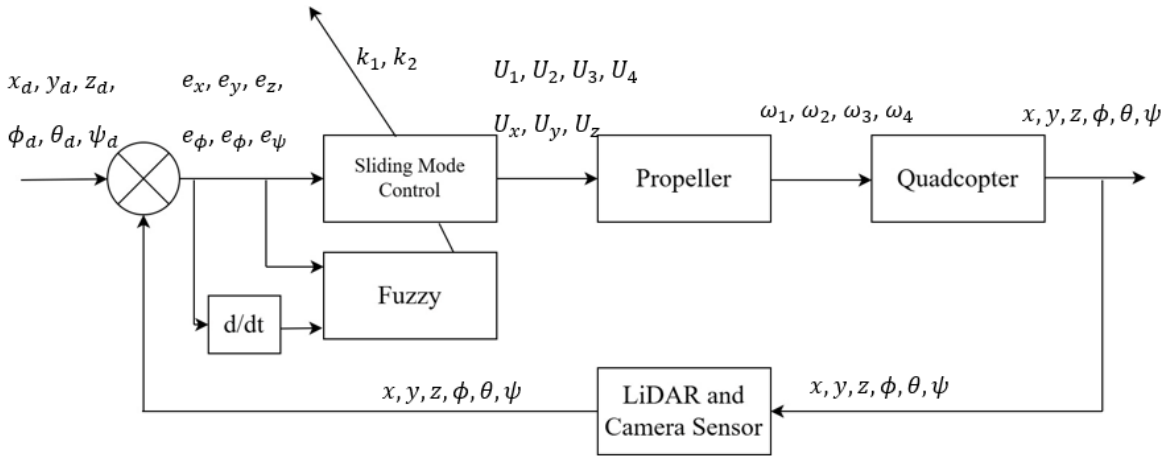

Fig. 3. Block diagram of control system

3. Results and Discussion

Determination of the path to be used will be assisted by camera sensor readings that will localize the indoor environment so that the path to be used will be mapped and the specified point can be reached by choosing the closest path to save time. At this stage, path planning is carried out in determining the destination point based on Fig. 4.

At first, the quadcopter is at one point which we consider as point (0,0) or the starting point. Then the quadcopter goes to the point to detect the cabinets to be addressed, so that recognition is carried out one by one at points A, B, C, and so on. 3D warehouse indoor environment design using Sketchup Pro 2020 software in the research that has been done according to Fig. 4. Fig. 5 is a 3D warehouse design with designed warehouse dimensions measuring 50 meters × 50 meters × 10

meters with a warehouse containing goods storage shelves. Thus, the quadcopter is simulated with conditions such as in real conditions.

The parameter values of the quadcopter used in the design are presented in Table 7. Subsequently, the quadcopter navigation system is obtained from the formulation of the trajectory equations (9) and (10). For the first result, it discusses the test simulation based on the dynamic modeling of the quadcopter system using Fuzzy-SMC control by providing feedback so that the RMSE plot can be carried out using MATLAB software.

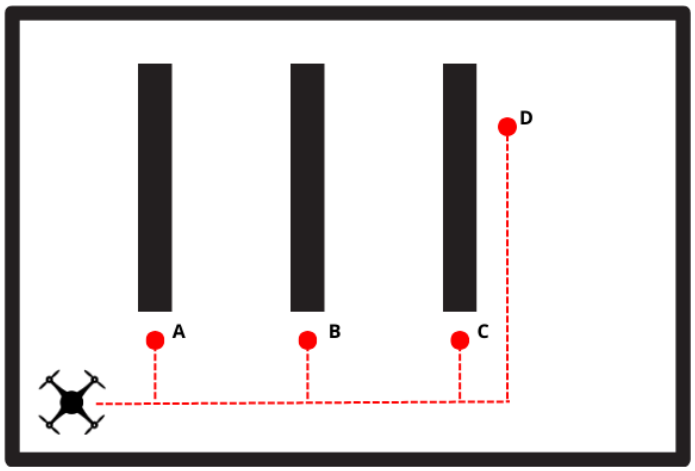

Fig. 4. Path planning of quadcopter

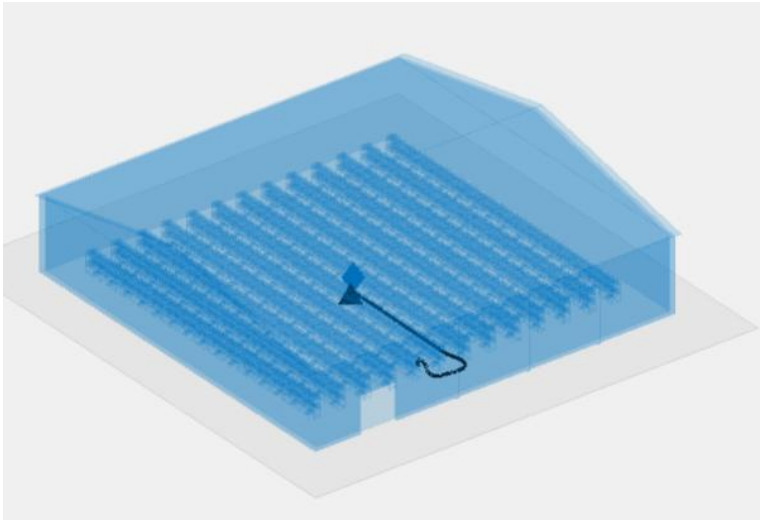

Fig. 5. 3D warehouse environment design

Table 7. Physical parameters of the quadcopter

No	Spesifikasi	Parameter	Unit	Value
1	Quadcopter mass	m	kg	1.75
2	Arm length to center of mass	l	m	0.25
3	Thrust coefficient	b	Ns^2	0.0107
4	Drag coefficient	k	Nms^2	0.78264×10^{-3}
5	Roll moment of inertia	I_{xx}	kgm^2	0.0133
6	Pitch moment of inertia	I_{yy}	kgm^2	0.0133
7	Yaw moment of inertia	I_{zz}	kgm^2	0.0214
8	Rotor moment of inertia	J	kgm^2	0.1021×10^{-6}

In Fig. 6 (a), the input is given in the form of the LiDAR sensor reading value, namely the x-position, then x-des as the input of the trajectory that the quadcopter will aim for. Thus, the reading

error is obtained. The error and delta error values obtained will be used as Fuzzy input for auto-tuning the Sliding Mode Control gain, as well as getting the sliding surface value in the form of S_x. Thus, from these inputs will get the x-axis position control marked with U_x. For the SMC gain value used depends on the delta error obtained from the feedback. Therefore, Fuzzy can provide output in the form of a gain value that matches the input in each condition, so that the chattering effect can be reduced. Then, modeling is also done for y-axis position control with input in the form of sensor readings, namely the y-axis. Thus, producing an output in the form of a U_y value using the control block in Fig. 6 (b). Then, in Fig. 6 (c), modeling is also done for z-axis position control with inputs in the form of z position reading values, desired values based on trajectory, and λ_z values. Thus, producing an output in the form of U_1 value.

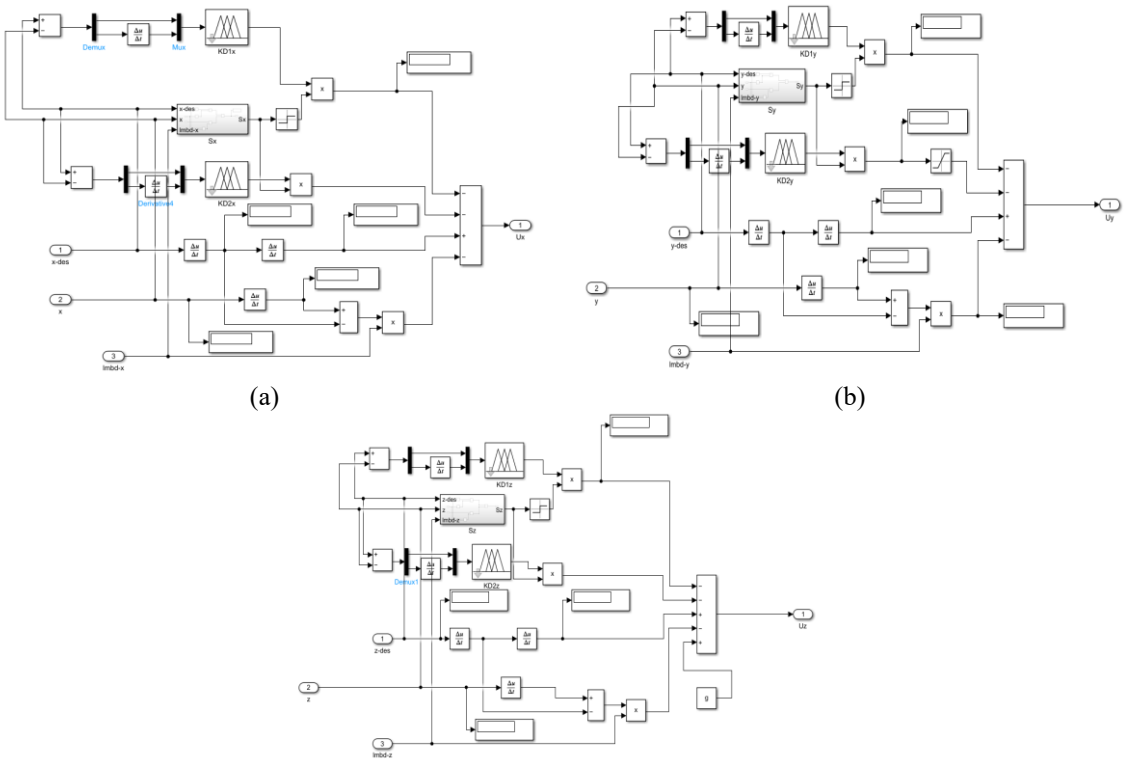

(a) (b)

(c)

Fig. 6. Position Control Block (a) x-Axis (b) y-Axis (c) z-Axis

First, a simulation was carried out using an SMC controller with constant gain values from the beginning to the end of the simulation. Based on the optimal tuning results, the values were obtained as k_1 = 42.01 and k_2 = 0.001. These tuned values were then implemented in the Simulink block, resulting in the test data presented in Fig. 7.

Subsequently, a simulation was conducted using parallel Fuzzy–Sliding Mode Control. Based on the position error readings, initialization was performed using Fuzzy logic, which acts as a tuner for the SMC parameters. The output of the Fuzzy system generates the gain values for the SMC. The resulting trajectory is shown in Fig. 7. using equation (9), a plot is made with the starting point [0 0 0], then moves on the z-axis or performs a flying mission with a height of 1.5 meters. Then proceed to move on the x-axis by 5 meters, and finally move on the y-axis by 10 meters. So, the quadcopter goes to the final destination point which is [5 10 1.5] according to Fig. 8. In trajectory variation A is a variation with a destination point of level 1 height on the warehouse shelf. Where, the determination of the height of the quadcopter is based on the midpoint of the height of the level 1 warehouse shelf.

Based on Fig. 8, the Fuzzy–Sliding Mode Control follows the predefined trajectory. However, in altitude control, an error is observed where the quadcopter does not reach the desired setpoint but remains below it. This occurs because, during the quadcopter's movement along the z-axis or take-off, a transition takes place from motion along the x-axis to motion along the z-axis, causing a change

in the gain value. Just as the gain value is about to be updated, the trajectory provides a control input to move along the x-axis. As a result Fig. 9, the quadcopter proceeds along the x-axis without reaching the desired altitude point. Consequently, the altitude is maintained at a constant level of 1.45 meters.

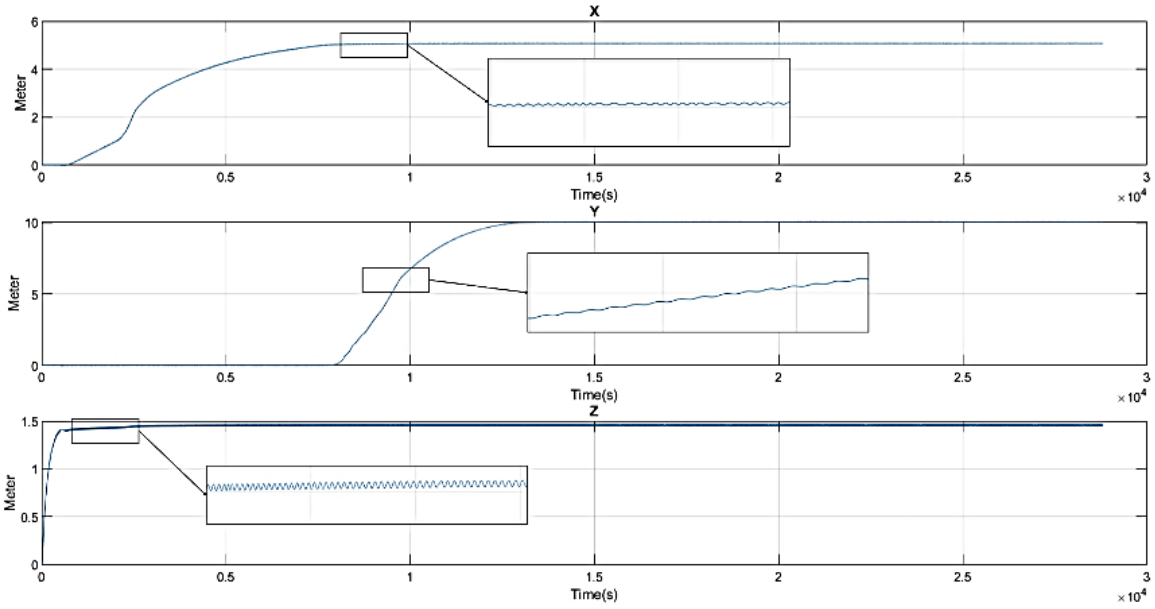

Fig. 7. Track test position data results I_A with SMC control

The average steady-state error values for LiDAR and camera sensor readings are presented in Table 8. The steady-state error is calculated once the quadcopter receives a constant input on the trajectory, indicating that it has reached the desired point. In this case, the error calculation is used to compare the performance of LiDAR and camera readings. Along the x-axis, the average steady-state error from the LiDAR sensor is higher than that of the camera, with values of 0.555% and 0.372%, respectively. For the y-axis, the error value cannot be calculated in this study because the simulation ended as the trajectory reached the desired point, resulting in no steady-state condition along the y-axis. Meanwhile, the average steady-state error on the z-axis shows 2.221% for LiDAR and 1.555% for the camera.

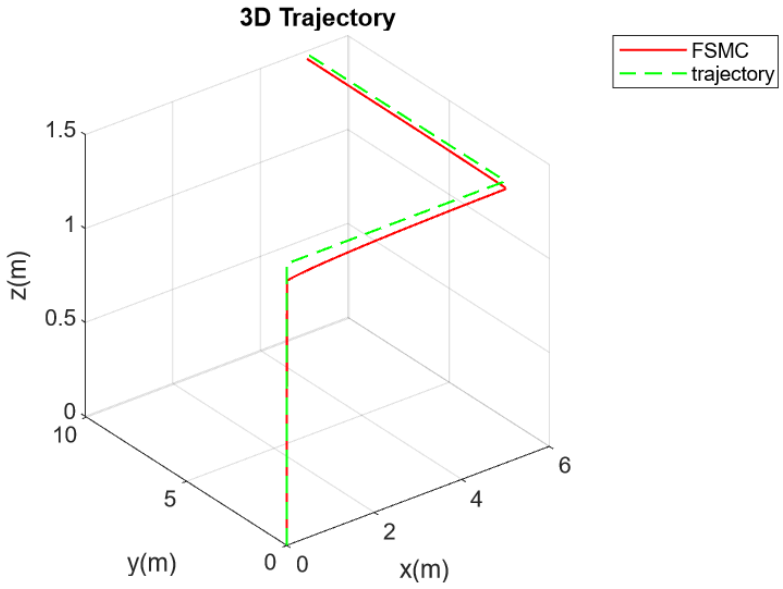

Fig. 8. 3D results of closed loop test trajectory I_A

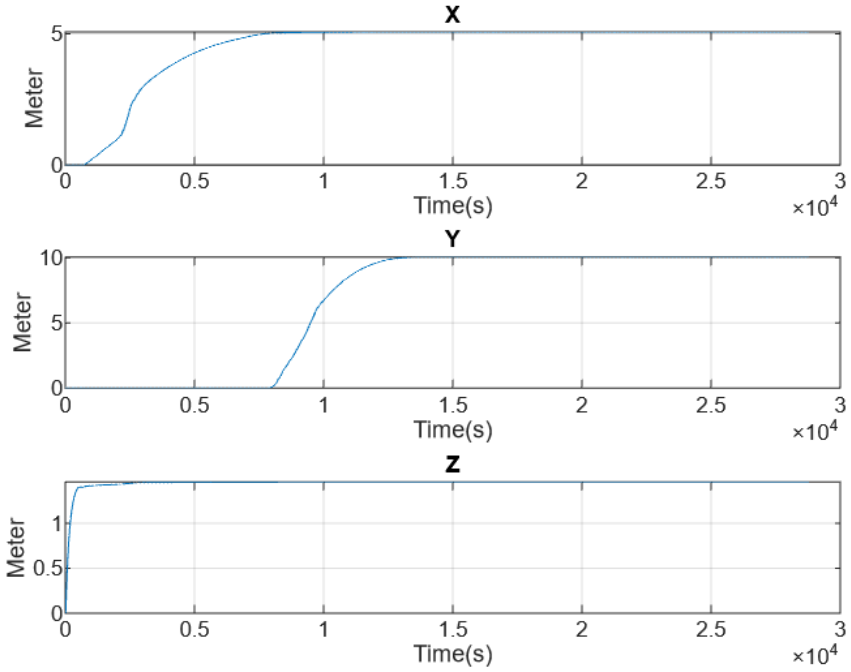

Fig. 9. Test position data results for trajectory I_A with Fuzzy–SMC

Table 8. Error value of I_A trajectory position after hovering

Average value of LiDAR Error (%)			Average value of Camera Error (%)		
x	y	z	x	y	z
0.555	0	2.221	0.372	0	1.555

Simulation results for the closed loop test on the I_B trajectory variation based on equation (10), plotting with the starting point [0 0 0], then moving on the z-axis or performing a flying mission with a height of 4.5 meters. Then proceed to move on the x-axis by 5 meters, and finally move on the y-axis by 10 meters. Thus, the quadcopter goes to the final destination point, namely [5 10 4.5]. In trajectory variation A is a variation with a destination point of level 2 height on the warehouse shelf. Based on Fig. 10, Fuzzy-SMC moves according to a predetermined trajectory. However, the height control shows an error, where the quadcopter does not touch the desired height, but less than the desired set point. This is because when the quadcopter moves on the z-axis or takes-off, in the transition condition from movement on the x-axis to movement towards the x-axis there is a change in the gain value. However, just as it is about to change its gain value, the trajectory provides control input to move on the x-axis. This causes the quadcopter to move on the x-axis without passing the desired altitude point. Therefore, the altitude is kept constant at 4.45 meters. Thus, the error data is obtained as in Table 9.

If we review the position based on time, as in Fig. 9 and Fig. 11, we can observe that at the beginning of the z-axis movement, there is a significant spike. However, when the quadcopter has not reached a height of 1.5 meters, the quadcopter is already moving in the x-axis. This is expected from the delay in providing control, and is thought to be caused by Fuzzy being too late to update the SMC gain value generated from fuzzification. The delay in changing the SMC gain value is due to the computation on the mamdani type Fuzzy which requires a longer computation time. This is because the rule base that is initiated is 7×7, where it will take longer to detect the input, output, and rule base values that are suitable for the current conditions.

Table 9. Error value of I_B trajectory position after hovering

Average value of LiDAR Error (%)			Average value of Camera Error (%)		
x	y	z	x	y	z
0.8	0	4.044	0.4	0	3.822

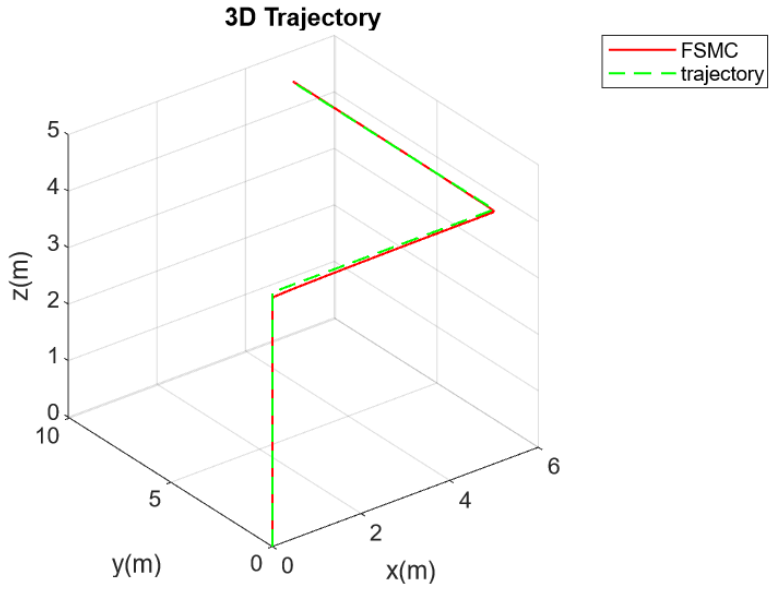

Fig. 10. 3D results of closed loop test of trajectory I_B

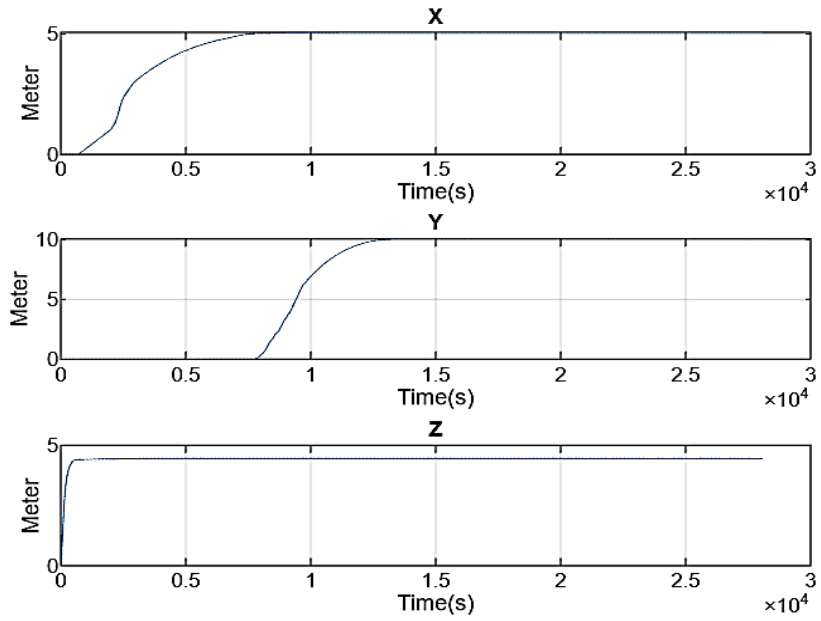

Fig. 11. Test track position data results for I_B with Fuzzy-SMC control

Table 9 shows the average value of steady state error for lidar and camera sensor readings when the quadcopter runs the mission on the I_B trajectory. The steady state error is calculated when the quadcopter has received constant input on the trajectory because it has reached its desired point. In this case, the error calculation is used to compare the lidar and camera readings. Based on the data in Table 9, for the x-axis, the average value of the lidar sensor reading error has a higher value than the camera, which is 0.8%, while the camera has an average error value of 0.4%. Then for the y-axis in this study, the error value cannot be calculated, this is because when the trajectory reaches the desired point, the simulation time ends, so the steady state on the y-axis does not exist. As for the average steady state error on the z-axis for lidar has an error of 4.044%, while the camera is 3.822%.

Based on the results in Table 8 and Table 9, it can be seen that the camera shows better accuracy compared to lidar. This is expected from the camera's ability to utilize more detailed visuals with pixel calculations in the initial condition compared to a certain condition very accurately. While lidar, has a lower performance because the simulation settings do not pay attention to factors such as laser reflection on uneven surfaces, material from obstacles in the form of cabinets that do not know

whether they absorb light or can affect the reflection of the rays emitted by LiDAR. In addition, the weather conditions are set to normal so that this position measurement should not be affected by weather conditions. Based on the results obtained, the difference between the lidar and camera sensor readings is 1-2 cm. When reviewing the location of the sensor mounting on the quadcopter, both are at the point [0 0 0], which is at the center of the body of the quadcopter

4. Conclusion

The indoor localization system was successfully developed by utilizing camera and LiDAR sensors to detect the quadcopter's position, where the camera demonstrated higher accuracy compared to LiDAR. The Fuzzy–SMC proved effective in maintaining stability and positional accuracy, as indicated by the average error on the X and Z axes ranging from 0 to 4.044% (below 5%), although the error value on the Y axis could not be calculated because the simulation stopped once the quadcopter reached its target point, preventing steady-state conditions from being observed. The main contribution of this study lies in the implementation of Fuzzy-SMC as an adaptive control approach capable of mitigating chattering effects while remaining robust against disturbances, making it relevant for supporting warehouse automation and similar industrial applications. Moving forward, simplifying the fuzzy rule base (e.g., 5×5 or 3×3) could be explored to reduce computational load, hardware-based implementation is needed to validate simulation results in real environments, and specific evaluation of the Y axis with longer simulation times is important to enable a more comprehensive analysis of system performance.

Author Contribution: All authors contributed equally to the main contributor to this paper. All authors read and approved the final paper.

Acknowledgment: The author is very grateful to the Sepuluh Nopember Institute of Technology for the contribution to the development of this scientific research with No: 2243/PKS/ITS/2025

Conflicts of Interest: The authors declare no conflict of interest.

References

[1] T. Dudek and K. Ka, "Optimizing drone logistics in complex urban industrial infrastructure ☆," *Transportation Research Part D: Transport and Environment*, vol. 140, p. 104610, 2025, https://doi.org/10.1016/j.trd.2025.104610.

[2] S. -C. Wu, W. -Y. Chiu and C. -F. Wu, "Deep Reinforcement Learning for Task Assignment and Shelf Reallocation in Smart Warehouses," *IEEE Access*, vol. 12, pp. 58915-58926, 2024, https://doi.org/10.1109/ACCESS.2024.3392752.

[3] Q. Zhao, X. Zhang and P. Wang, "Multi-Type Equipment Selection and Quantity Decision Optimization in Intelligent Warehouse," *IEEE Access*, vol. 12, pp. 63515-63527, 2024, https://doi.org/10.1109/ACCESS.2024.3395288.

[4] S. M. Tabatabaei, "Sustainable supply chain network design: Integrating risk management, resilient multimodal transportation, and production strategy," *Journal of Industrial Information Integration*, vol. 47, p. 100897, 2025, https://doi.org/10.1016/j.jii.2025.100897.

[5] I. H. Mohamud, M. Abdul Kafi, S. A. Shahron, N. Zainuddin, and S. Musa, "The Role of Warehouse Layout and Operations in Warehouse Efficiency: A Literature Review," *Journal Européen des Systèmes Automatisés*, vol. 56, no. 1, pp. 61-68, 2023, https://doi.org/10.18280/jesa.560109.

[6] W. Larutama, D. R. Bentar, R. O. Risdayanto, and R. S. Alvariedz, "Implementation of Warehouse Management System Planning in Finished Goods Warehouse," *Journal of Logistics and Supply Chain*, vol. 2, no. 2, pp. 81-90, 2022, https://doi.org/10.17509/jlsc.v2i2.62840.

[7] Y. Guo, F. Liu, J. S. Song, and S. Wang, "Supply chain resilience: A review from the inventory management perspective," *Fundamental Research*, vol. 5, no. 2, pp. 450-463, 2024,

https://doi.org/10.1016/j.fmre.2024.08.002.

[8] E. Arunadevi and S. Umamaheswari, "Enhancing ameliorating items with sustainable inventory management strategies: A Weibull approach for time and price-dependent demand trends," *Ain Shams Engineering Journal*, vol. 15, no. 12, p. 103065, 2024, https://doi.org/10.1016/j.asej.2024.103065.

[9] W. Villegas-ch, A. Maldonado, and S. Sanchez-viteri, "Intelligent Systems with Applications Optimization of inventory management through computer vision and machine learning technologies," *Intelligent Systems with Applications*, vol. 24, p. 200438, 2024, https://doi.org/10.1016/j.iswa.2024.200438.

[10] S. Teck, T. S. Phạm, L. M. Rousseau, and P. Vansteenwegen, "Deep reinforcement learning for the real-time inventory rack storage assignment and replenishment problem," *European Journal of Operational Research*, vol. 327, no. 2, pp. 606-622, 2025, https://doi.org/10.1016/j.ejor.2025.05.008.

[11] A. Zarinchang, K. Lee, I. Avazpour, J. Yang, D. Zhang, and G. K. Knopf, "Adaptive warehouse storage location assignment with considerations to order-picking efficiency and worker safety," *Journal of Industrial and Production Engineering*, vol. 41, no. 1, pp. 40-59, 2024, https://doi.org/10.1080/21681015.2023.2263009.

[12] S. Dalla, C. Bellochio, and P. Carteri, "Occupational hazards at grain pre-processing and storage facilities: A review," *Journal of Stored Products Research*, vol. 106, p. 102288, 2024, https://doi.org/10.1016/j.jspr.2024.102288.

[13] Y. Xiang, K. Wang, and X. Wu, "Matching of manual operation trajectories and warehouse operation information: A data chain Construction method based on indoor positioning technology," *Expert Systems with Applications*, vol. 274, p. 127016, 2025, https://doi.org/10.1016/j.eswa.2025.127016.

[14] D. Almaskati, S. Kermanshachi, A. Pamidimukkala, K. Loganathan, and Z. Yin, "A Review on Construction Safety: Hazards, Mitigation Strategies, and Impacted Sectors," *Buildings*, vol. 14, no. 2, p. 526, 2024, https://doi.org/10.3390/buildings14020526.

[15] S. Yu and S. Srinivas, "Collaborative Human–Robot Teaming for Dynamic Order Picking: Interventionist strategies for improving warehouse intralogistics operations," *Transportation Research Part E: Logistics and Transportation Review*, vol. 197, p. 104082, 2025, https://doi.org/10.1016/j.tre.2025.104082.

[16] World Health Organization, "Occupational safety and health in public health emergencies," *World Health Organization*, 2018, https://apps.who.int/iris/bitstream/handle/10665/275385/9789241514347-eng.pdf?ua=1&ua=1.

[17] X. Lyu, "Intelligent warehousing performance management based on Internet of Things and automation technology in the context of green manufacturing," *Thermal Science and Engineering Progress*, vol. 53, p. 102761, 2024, https://doi.org/10.1016/j.tsep.2024.102761.

[18] S. Hina, Q. Abbas, and K. Ahmed, "Adversarial attacks on artificial Intelligence of Things-based operational technologies in theme parks," *Internet of Things*, vol. 32, p. 101654, 2025, https://doi.org/10.1016/j.iot.2025.101654.

[19] N. Xu, M. Guan, and C. Wen, "A survey on Ultra Wide Band based localization for mobile autonomous machines," *Journal of Automation and Intelligence*, vol. 4, no. 2, pp. 82-97, 2025, https://doi.org/10.1016/j.jai.2025.02.001.

[20] S. Fadil, I. Sebari, M. A. Moulay, and K. A. El kadi, "Modeling and spatialization of biomass and carbon stock using unmanned Aerial Vehicle Lidar (Lidar-UAV) metrics and forest inventory in cork oak forest of Maamora," *Regional Science Policy & Practice*, vol. 16, no. 11, p. 100127, 2024, https://doi.org/10.1016/j.rspp.2024.100127.

[21] A. Daios, A. Xanthopoulos, D. Folinas, and I. Kostavelis, "Towards automating stocktaking in warehouses: Challenges, trends, and reliable approaches," *Procedia Computer Science*, vol. 232, no. 2023, pp. 1437-1445, 2024, https://doi.org/10.1016/j.procs.2024.01.142.

[22] M. Golam, M. F. Rahaman, M. R. Subhan, D.-S. Kim, and J.-M. Lee, "BUS-Health: Blockchain and UAV Integrated Smart Medical Supplies," *Blockchain: Research and Applications*, p. 100341, 2025, https://doi.org/10.1016/j.bcra.2025.100341.

[23] J. S. Bulhões *et al*., "Control and stabilization of quadcopters subjected to propeller failures," *Robotics and Autonomous Systems*, vol. 194, p. 105162, 2025, https://doi.org/10.1016/j.robot.2025.105162.

[24] J. A. Marshall, W. Sun, and A. L'Afflitto, "A survey of guidance, navigation, and control systems for autonomous multi-rotor small unmanned aerial systems," *Annual Reviews in Control*, vol. 52, pp. 390-427, 2021, https://doi.org/10.1016/j.arcontrol.2021.10.013.

[25] X. Tong, X. Xiao, X. Jin, and H. Wang, "Nonlinear adaptive estimator-based prescribed performance control of perturbed quadcopter systems," *Applied Mathematics and Computation*, vol. 509, p. 129663, 2026, https://doi.org/10.1016/j.amc.2025.129663.

[26] A. Eltayeb *et al*., "Challenges in Multi-domain Robot Swarm for Industrial Mapping and Asset Monitoring," *Transportation Research Procedia*, vol. 84, pp. 534-542, 2025, https://doi.org/10.1016/j.trpro.2025.03.106.

[27] C. Gao *et al*., "A UAV-based explore-then-exploit system for autonomous indoor facility inspection and scene reconstruction," *Automation in Construction*, vol. 148, p. 104753, 2023, https://doi.org/10.1016/j.autcon.2023.104753.

[28] J. Li, X. Xiong, Y. Yan and Y. Yang, "A Survey of Indoor UAV Obstacle Avoidance Research," *IEEE Access*, vol. 11, pp. 51861-51891, 2023, https://doi.org/10.1109/ACCESS.2023.3262668.

[29] Y. Li, Q. Wang, Z. Hao, S. Hu, J. Wu, and L. Dong, "IRAL: Robust and versatile UAV localization using infrared vision and altitude sensor fusion," *Measurement*, vol. 242, p. 115917, 2025, https://doi.org/10.1016/j.measurement.2024.115917.

[30] D. Lei, L. Luo, S. Chen and W. Li, "PL-ALF: A Novel Point-Line Feature Autonomous Localization and Flight Framework Based on Multisensor Fusion and Optimization," *IEEE Transactions on Instrumentation and Measurement*, vol. 74, pp. 1-15, 2025, https://doi.org/10.1109/TIM.2024.3522670.

[31] S. Wang and N. S. Ahmad, "AI-based approaches for improving autonomous mobile robot localization in indoor environments: A comprehensive review," *Engineering Science and Technology, an International Journal*, vol. 63, p. 101977, 2025, https://doi.org/10.1016/j.jestch.2025.101977.

[32] Y. He and X. He, "Research on an Improved Stepwise Feature Matching Algorithm for UAV Indoor Localization," *IEEE Access*, vol. 13, pp. 67323-67333, 2025, https://doi.org/10.1109/ACCESS.2025.3559989.

[33] K. Wang, L. Kooistra, Y. Wang, S. Vélez, W. Wang, and J. Valente, "Benchmarking of monocular camera UAV-based localization and mapping methods in vineyards," *Computers and Electronics in Agriculture*, vol. 227, p. 109661, 2024, https://doi.org/10.1016/j.compag.2024.109661.

[34] J. V. -V. Gerwen, K. Geebelen, J. Wan, W. Joseph, J. Hoebeke and E. De Poorter, "Indoor Drone Positioning: Accuracy and Cost Trade-Off for Sensor Fusion," *IEEE Transactions on Vehicular Technology*, vol. 71, no. 1, pp. 961-974, 2022, https://doi.org/10.1109/TVT.2021.3129917.

[35] H. Y. Lin, K. L. Chang, and H. Y. Huang, "Development of Unmanned Aerial Vehicle Navigation and Warehouse Inventory System Based on Reinforcement Learning," *Drones*, vol. 8, no. 6, p. 220, 2024, https://doi.org/10.3390/drones8060220.

[36] P. Chhikara, R. Tekchandani, N. Kumar, V. Chamola and M. Guizani, "DCNN-GA: A Deep Neural Net Architecture for Navigation of UAV in Indoor Environment," *IEEE Internet of Things Journal*, vol. 8, no. 6, pp. 4448-4460, 2021, https://doi.org/10.1109/JIOT.2020.3027095.

[37] C. Li *et al*., "ReLoc 2.0: UHF-RFID Relative Localization for Drone-Based Inventory Management," *IEEE Transactions on Instrumentation and Measurement*, vol. 70, pp. 1-13, 2021, https://doi.org/10.1109/TIM.2021.3069377.

[38] A. Yusefi, A. Durdu, M. F. Aslan and C. Sungur, "LSTM and Filter Based Comparison Analysis for Indoor Global Localization in UAVs," *IEEE Access*, vol. 9, pp. 10054-10069, 2021, https://doi.org/10.1109/ACCESS.2021.3049896.

[39] S. Wang and N. S. Ahmad, "A Comprehensive Review on Sensor Fusion Techniques for Localization of a Dynamic Target in GPS-Denied Environments," *IEEE Access*, vol. 13, pp. 2252-2285, 2025, https://doi.org/10.1109/ACCESS.2024.3519874.

[40] C. Sandamini *et al*., "A Review of Indoor Positioning Systems for UAV Localization with Machine Learning Algorithms," *Electronics*, vol. 12, no. 7, p. 1533, 2023, https://doi.org/10.3390/electronics12071533.

[41] H. Chen, L. Zhang, D. Li, J. Xu, W. Yang and Z. Yang, "REFLoc: A Resilient Evolutionary Fusion Framework for Robust Indoor Localization," *IEEE Transactions on Instrumentation and Measurement*, vol. 73, pp. 1-13, 2024, https://doi.org/10.1109/TIM.2024.3403196.

[42] M. Idrissi, M. Salami, and F. Annaz, "A Review of Quadrotor Unmanned Aerial Vehicles: Applications, Architectural Design and Control Algorithms," *Journal of Intelligent & Robotic Systems*, vol. 104, no. 2, 2022, https://doi.org/10.1007/s10846-021-01527-7.

[43] R. Ferede, G. de Croon, C. De Wagter, and D. Izzo, "End-to-end neural network based optimal quadcopter control," *Robotics and Autonomous Systems*, vol. 172, p. 104588, 2024, https://doi.org/10.1016/j.robot.2023.104588.

[44] A. Khan, A. Waqar, B. Kim, and D. Park, "A review on recent advances in sound source localization techniques, challenges, and applications," *Sensors and Actuators Reports*, vol. 9, p. 100313, 2025, https://doi.org/10.1016/j.snr.2025.100313.

[45] S. Xu, L. Zhang, X. Wang, J. Chen, F. Wei and Y. Wu, "Indoor Cooperative Localization for a Swarm of Micro UAVs Based on Visible Light Communication," *IEEE Systems Journal*, vol. 17, no. 4, pp. 6504-6515, 2023, https://doi.org/10.1109/JSYST.2023.3312279.

[46] P. Zhao, H. Zhang, G. Liu, X. Cui, and M. Lu, "A UWB-AOA / IMU Integrated Navigation System for 6-DoF Indoor UAV Localization," *Drones*, vol. 9, no. 8, p. 546, 2025, https://doi.org/10.3390/drones9080546.

[47] S. Boiteau, F. Vanegas, J. Galvez-Serna, and F. Gonzalez, "Model-Based RL Decision-Making for UAVs Operating in GNSS-Denied, Degraded Visibility Conditions with Limited Sensor Capabilities," *Drones*, vol. 9, no. 6, p. 410, 2025, https://doi.org/10.3390/drones9060410.

[48] H. Wu, W. Wang, T. Wang, and S. Suzuki, "Sliding Mode Control Approach for Vision-Based High-Precision Unmanned Aerial Vehicle Landing System Under Disturbances," *Drones*, vol. 9, no. 1, p. 3, 2025, https://doi.org/10.3390/drones9010003.

[49] P. A. Darwito and K. D. Wahyuadnyana, "Performance Examinations of Quadrotor with Sliding Mode Control-Neural Network on Various Trajectory and Conditions," *Mathematical Modelling of Engineering Problems*, vol. 9, no. 3, pp. 707-714, 2022, https://doi.org/10.18280/mmep.090317.

[50] N. P. Agustina, P. A. Darwito, B. L. Widjiantoro, and M. Raditya, "Stability Control of Multi-Quadcopter Formation Based on Virtual Leader and Flocking Algorithm," *Journal of Robotics and Control (JRC)*, vol. 6, no. 3, pp. 1187-1196, 2025, https://doi.org/10.18196/jrc.v6i3.25598.

[51] Y. Jing, A. Mirza, and R. Sipahi, J. Martinez-Lorenzo, "Sliding Mode Controller with Disturbance Observer for Quadcopters; Experiments with Dynamic Disturbances and in Turbulent Indoor Space," *Drones*, vol. 7, no. 5, p. 328, 2023, https://doi.org/10.3390/drones7050328.

[52] A. Eltayeb, M. F. Rahmat, M. A. M. Basri, M. A. M. Eltoum and S. El-Ferik, "An Improved Design of an Adaptive Sliding Mode Controller for Chattering Attenuation and Trajectory Tracking of the Quadcopter UAV," *IEEE Access*, vol. 8, pp. 205968-205979, 2020, https://doi.org/10.1109/ACCESS.2020.3037557.

[53] M. A. Sepestanaki, M. H. Barhaghtalab, S. Mobayen, A. Jalilvand, A. Fekih and P. Skruch, "Chattering-Free Terminal Sliding Mode Control Based on Adaptive Barrier Function for Chaotic Systems With Unknown Uncertainties," *IEEE Access*, vol. 10, pp. 103469-103484, 2022, https://doi.org/10.1109/ACCESS.2022.3209993.

[54] T. R. D. Kumar and S. J. Mija, "Boundary Logic-Based Hybrid PID-SMC Scheme for a Class of Underactuated Nonlinear Systems-Design and Real-Time Testing," *IEEE Transactions on Industrial Electronics*, vol. 72, no. 5, pp. 5257-5267, 2025, https://doi.org/10.1109/TIE.2024.3456003.

[55] F. Hu, T. Ma and X. Su, "Adaptive Fuzzy Sliding-Mode Fixed-Time Control for Quadrotor Unmanned Aerial Vehicles With Prescribed Performance," *IEEE Transactions on Fuzzy Systems*, vol. 32, no. 7, pp. 4109-4120, 2024, https://doi.org/10.1109/TFUZZ.2024.3393763.

[56] H. D. Choi, K. S. Kim, P. Shi and C. K. Ahn, "Adaptive Neuro-Fuzzy Sliding Mode Tracking for Quadrotor UAVs," *IEEE Transactions on Automation Science and Engineering*, vol. 22, pp. 16322-16333, 2025, https://doi.org/10.1109/TASE.2025.3576292.

[57] H. B. Meharie and L. N. Lemma, "Optimized Robust Fuzzy Twisting Sliding Mode Control Design for Fixed Wing UAV," *IEEE Access*, vol. 12, pp. 170112-170134, 2024, https://doi.org/10.1109/ACCESS.2024.3497723.

[58] M. M. Beharie, J. O. Pedro, L. Dala, "Design of a quadrotor flight test stand for system identification," *The Aeronautical Journal*, vol. 119, no. 1214, pp. 501-521, 2015, https://doi.org/10.1017/S0001924000010587.

[59] A. Eltayeb, M. F. Rahmat, M. A. M. Basri, M. A. M. Eltoum and M. S. Mahmoud, "Integral Adaptive Sliding Mode Control for Quadcopter UAV Under Variable Payload and Disturbance," *IEEE Access*, vol. 10, pp. 94754-94764, 2022, https://doi.org/10.1109/ACCESS.2022.3203058.

[60] M. Mohammadinodoushan, R. Abbassi, H. Jerbi, F. Waly Ahmed, H. Abdalqadir kh ahmed, and A. Rezvani, "A new MPPT design using variable step size perturb and observe method for PV system under partially shaded conditions by modified shuffled frog leaping algorithm- SMC controller," *Sustainable Energy Technologies and Assessments*, vol. 45, p. 101056, 2021, https://doi.org/10.1016/j.seta.2021.101056.

[61] P. A. Darwito and N. P. Agustina, "Performance Evaluation of a Sliding Mode Control-Kalman Filter-Based Mathematical Model for Altitude and Attitude Control in Quadcopters," *Journal of Intelligent Systems and Control*, vol. 2, no. 2, pp. 70-81, 2023, https://doi.org/10.56578/jisc020202.

[62] N. P. Agustina and P. A. Darwito, "Autonomous Quadcopter Trajectory Tracking and Stabilization Using Control System Based on Sliding Mode Control and Kalman Filter," *2023 International Seminar on Intelligent Technology and Its Applications (ISITIA)*, pp. 489-493, 2023, https://doi.org/10.1109/ISITIA59021.2023.10221176.